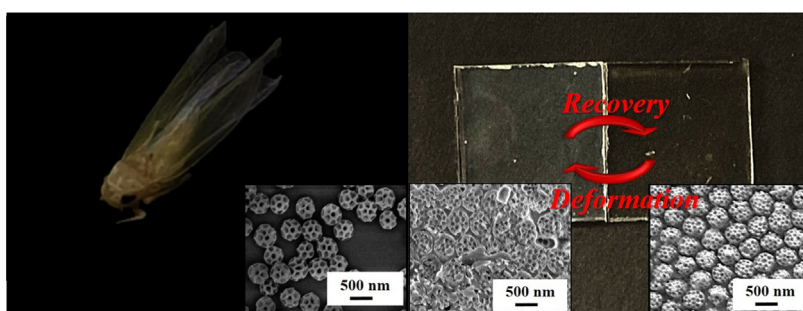Regular Article

Reversible embroidered ball-like antireflective structure arrays inspired by leafhopper wings

Pei-Chun Li, Huei-Yin Chen, Kuan-Ting Chiang, Hongta Yang *

Department of Chemical Engineering, National Chung Hsing University, 145 Xingda Road, Taichung City 40227, Taiwan

GRAPHICAL ABSTRACT

ARTICLE INFO

ABSTRACT

Highly transparent leafhopper (*Thaia rubiginosa*) wings are self-decorated with embroidered ball-shaped proteinaceous brochosmoes as distinct anti-predator defenses. The non-sticky brochosomal coating serves as antireflective structures for camouflage in vegetated environments. Inspired by the leafhopper wings, this study reports a new type of reversible antireflection coating enabled by integrating self-assembly methodologies using a shape memory polymer. The resulting embroidered ball-like structure array establishes a refractive index transition on surface, and thereby behaves omnidirectional antireflective characteristics in a broadband visible light region. Interestingly, the highly transparent appearance can be instantly erased and recovered by submerging in common liquids, such as water and ethanol, or by applying contact pressures at ambient conditions. Furthermore, the reversibility and structure-shape effect on the antireflective characteristics are systematically evaluated in this study.

© 2021 Elsevier Inc. All rights reserved.

1. Introduction

Owing to a refractive index mismatch, Fresnel reflection appears as light propagates through two different media [1]. The stray light reflection at the media interface, accompanied by energy loss, results in veil glare, low visible transmittance, and deteriorated contrast on optical instruments and devices. To eliminate the vision impairments, a variety of polymer films have been extensively employed to render destructive interferences [2–4]. Unfortunately, single-layer antireflection coatings suffer from rare choices of low-refractive-index polymers, and are limited by narrowband antireflection performance. Even though appropriately designed multilayer antireflection coatings can minimize light reflection over a broad wavelength region, there are challenges associated with poor thermal stability and mechanical properties between foreign polymers [5–7]. To address the issues, a wide spectrum of inorganic materials are employed to introduce porosity in antireflection coatings through stacking inorganic particles, integration of voids using inorganic hollow particles, and

multilayer depositions of high and low refractive index inorganic materials [8–10]. For uniformly dense inorganic particles, the porosity can be controlled to reduce the apparent refractive index by changing the packing arrangement and the particle diameter [11]. Nevertheless, there is a practical limit on particle diameter for the reason that large particles scatter visible light. Although the same concept is evident on porous antireflection coatings consisting of inorganic hollow particles, large-scale processes for fabricating the hollow particles are rare [12]. Most processes developed to date are multistep, and require large amounts of surfactants, which leads to poor mechanical properties. Compared with that, mechanically robust multilayer antireflection coatings allow reduction of optical reflection even for a broad wavelength region [13]. However, multiple depositions of inorganic materials increase the fabrication costs, and therefore the coating are solely applied in high end markets.

Living creatures on earth, such as moths, long-tail glasswing butterflies, and cicadas, have created graded refractive indices over sufficient heights on compound eyes or wing surfaces for suppressing optical reflection and light scattering [14–16]. Taking the surface architectures of nature as prototypes, booming researches have attempted to emulate the intricate antireflective structures over four billion years of evolution. In recent years, numerous submicrometer-scale structure arrays, including but not limited to dome-shaped structure arrays, conical structure arrays, pyramid-like structure arrays, and nipple-shaped structure arrays, are developed to serve as antireflection structures [17–23]. However, most structures with high aspect ratios are established by exploiting lithography-based fabrication technologies, which are restricted to low-resolution features and dedicated instruments along with complicated processing steps. On the contrary, self-assembly methodologies render a simple and inexpensive alternative to develop submicrometer-scale colloidal crystals, hole arrays, and so on [24–26]. Nevertheless, the self-assembled structures suffer from insufficient depths and abrupt refractive index transitions, resulting in less prominent antireflection performances, especially at large incidence angles [27–28]. Unlike the early discovery of natural antireflective architectures, small yellow leafhoppers secrete non-sticky proteinaceous brochosomes on wings to camouflage themselves without extensive coloration [29,30]. These embroidered ball-shaped brochosomes create a refractive index transition on the wing surfaces to prevent them from being reflective. The astonishing nearly invisible appearance allows the leafhoppers to vanish into their surroundings, and to protect against predators. Unfortunately, current micro/nanomanufacturing technologies to engineer submicrometer-scale embroidered ball-like structures of various geometries have been rare [31]. Although the artificial brochosomes fabricated through electrochemical deposition of metals on double-layer colloidal crystal templates greatly enhance omnidirectional antireflection performance, the metal brochosome-covered substrate becomes dark in color.

To date, reversible antireflection coatings have realized growing performance demands of numerous applications in architectural partitions, vehicle windows, display screens, and optical lenses [32–34]. The antireflective structures can be deformed and reconstructed under specific environmental conditions, making it possible to completely reverse the antireflective characteristics. Nevertheless, studies focused on fabricating the intelligent coatings have been rare [35,36]. Additionally, the adopted solvent-induced phase transformations of polyelectrolyte multilayers and copolymers are incompatible with environments, and limited by short-term applications. In recent years, prosperous inventions of shape memory polymers, which are capable of altering polymer chain configurations in response to various external stimuli, have been exploited to modulate biomimetic structural color materials [37–41]. The conventional shape memory polymers are divided into chemical-stimuli-responsive polymers and physical-stimuli-responsive polymers. Permanent structures of either polymers can be mechanically deformed above glass transition temperatures, and then frozen after cooling below the temperatures. The temporary configurations are finally recovered to their permanent structures through increasing polymer chain mobility, triggered by applying external chemical stimuli or physical stimuli. Thanks to the progressive inventions, integration of the promising shape memory polymers and structure arrays may provide a platform for implementing prospective intelligent antireflection coatings. However, the heat-demanding structure transformations employed by the existing shape memory polymers greatly impede the ultimate performances for meeting broad application requirements [42]. Moreover, chemical-stimuli-responsive structural recoveries generally make use of particular organic solutions, which corrode other device elements and possess adverse effects on human health [43]. On the contrary, physical stimuli, including heat, ultraviolet radiations, electromagnetic fields, and mechanical forces, can also be exploited to overcome resistances of the shape memory polymers against externally applied deformations [44–46]. Unfortunately, physical-stimuli-responsive structural recoveries are hindered by longer recovery periods, which are not suitable to numerous applications that desire rapid responses.

Herein, a novel variety of shape memory polymer is presented in this work. The material configuration is capable of instantaneously switching between a permanent and temporary state at ambient conditions. Integration of the shape memory polymer and embroidered ball-like structure arrays, inspired by leafhopper-generated brochosomal coatings, enables the development of deformable antireflective structures. The structures can be reversibly transformed by applying contact pressures and exposure to low surface tension solvents even after removing the stimuli, resulting in a reversible antireflective characteristic over wide viewing angles. Importantly, the non-lithography-based fabrication approach allows the preparation of large-area intelligent optical applications.

2. Experimental section

2.1. Materials and reagents

Small yellow leafhopper (*Thaia rubiginosa*) specimens are provided by Taiwan Insect Museum, and analyzed without any further treatment. The reagents applied for StÖber silica colloid synthesis consist of 200 proof anhydrous ethanol (Echochemical Corporation), ammonium hydroxide (Sigma-Aldrich), tetraethyl orthosilicate (Sigma-Aldrich), and ultrapure deionized water (Milli-Q system). The materials include ethoxylated trimethylolpropane triacrylate (ETPTA) monomer (Sartomer Company Corporation), 2-hydroxy-2-methyl-1-phenyl-1-propanone (HMPP) (BASF Corporation), perfluoropolyether methacrylate (PFPE-MAA) monomer (Exfluor Research Corporation), and ethylene glycol diacrylate (EGDA) monomer (Sartomer Company Corporation), are introduced to engineer polymeric templates and structure arrays. Hydrofluoric acid aqueous solution is purchased from Sigma-Aldrich. Glass microscope slides acquired from Thermo Fisher Scientific are rinsed with a mixture of anhydrous ethanol and ultrapure deionized water before use.

2.2. Self-assembly of close-packed hole arrays

Well-established StÖber process is employed to synthesize monodispersed spherical silica colloids with tunable diameters (90, 300, 450, and 600 nm) [47]. As indicated in previous work, the silica colloids are dispersed in PEPE-MMA monomers, in which

the colloid volume fraction of the suspension can be adjusted from 20 vol% to 40 vol% [48]. A modified Langmuir-Blodgett technology is developed to self-assemble hole arrays. In the self-assembly process, a rinsed glass microscope slide adhered to a K_D Scientific syringe pump is immersed in ultrapure deionized water. The PFPE-MAA monomer/silica colloidal suspension is dripped on the water surface, during which the PFPE-MAA monomer-covered colloids speedily spread and spontaneously assemble into a close-packed monolayer. The floating colloidal monolayer is then continuously deposited on the glass slide by withdrawing that with a constant velocity of 3 mm/*sec* using the syringe pump. The monomers are capable of flowing and filling the voids between the colloid crystals and the glass slide. After UV-polymerizing the monomers for a few seconds in OPAS XLite™ 500 UV curing systems, the silica colloids embedded in poly(PFPE-MAA) matrices are wet-etched using a hydrofluoric acid aqueous solution (1 vol%) to pattern a close-packed hole array.

2.3. Templating fabrication of embroidered ball-like structure arrays

Nanometer-scale silica colloids are dispersed in ETPTA monomers consisting of HMPP (1 vol%) to prepare an ETPTA monomer/silica colloidal suspension, in which the colloid volume fraction is controlled to be 20 vol%. The ETPTA monomer-covered colloids are self-assembled using the above-mentioned Langmuir-Blodgett technology, and then transferred onto the as-patterned hole array. After UV-polymerization of the ETPTA monomers, the nanometer-scale silica colloid-coated hole array can serve as a second-generation template. In the templating fabrication procedure, a mixture of ETPTA monomer (25 vol%), EGDA monomer (74 vol%), and HMPP (1 vol%) is poured onto the template and degassed for 10 min to eliminate any trapped air. The monomer mixture is then UV-polymerized, allowing it to be peeled off from the hole array. The embedded nanometer-scale silica colloids are subsequently removed to engineer an embroidered ball-like structure array.

2.4. Characterization

Photographic images and surface morphologies of specimens are carried out by a Carnon SX740 digital camera and a JEOL 6335F scanning electron microscopy (SEM), respectively. Prior to SEM imaging, the specimens are sputter-coated with a platinum layer. Reflectance and transmittance spectra in the visible spectral range are conducted by an Ocean Optics HR4000 UV–visible-NIR spectrometer using a halogen tungsten light source.

3. Results and discussion

Highly transparent small yellow leafhopper (*Thaia rubiginosa*) wings exhibit low reflectance (ca. 7%) and high transmittance (ca. 91%) in the whole visible spectral range at normal incidence (Fig. 1 (a) and 1 (b)). The low reflectivity originates from leafhopper-produced secretory brochosomal coatings (Fig. 1 (c)). The embroidered ball-like brochosomes create a gradual refractive index transition on the wing surface for greatly suppressing incident light reflection in a broadband visible wavelength range. It is worth to mention that the wings are mainly composed of chitin, which do not absorb visible light [49,50]. The energy loss (2%) is attributed to the presence of light scattering. In comparison with that, the average reflectance and average transmittance of the leafhopper wings are increased by ca. 8% and decreased by ca. 11%, respectively, after rubbing out the non-sticky brochosomes under bath-type ultrasonication (400 Watts) for 10 min (Fig. 1 (d)). It is worthwhile to note that the difference between increased average reflectance and decreased average transmittance is attributed to light scattering and light absorption by the uncovered wings. The findings further demonstrate the antireflective characteristics of the embroidered ball-like brochosomes.

Inspired by the small yellow leafhopper wings, artificial brochosome arrays are engineered through integrating a modified Langmuir-Blodgett technology and a templating method. As illustrated in Fig. 2, submicrometer-scale PFPE-MAA monomer-covered silica colloids are self-assembled into a close-packed monolayer on water surface, induced by large surface tension difference between PFPE-MAA monomer and water, and then transferred onto a glass substrate. The monomers are capable of flowing and filling the voids between the silica colloid crystals and the glass substrate, caused by capillary actions and gravitational forces. After UV-polymerization, the silica colloids embedded in the poly(PFPE-MAA) matrix are wet-etched to pattern a close-packed hole array. The roll-to-roll compatible Langmuir-Blodgett technology is ready for scale-up to deposit self-assembled colloid crystals of several hundred square centimeters [51,52]. Afterward, monolayer nanometer-scale ETPTA monomer-covered silica colloid crystals are deposited on the as-patterned hole array using the above-mentioned methodology (Fig. S1). By repeating the self-assembly procedure, multilayer silica colloid crystals can be created, while the ETPTA monomer functions as an adhesive in the procedure. A mixture of ETPTA monomer, EGDA monomer, and HMPP with appropriate amount is subsequently poured onto the silica colloidal crystal-deposited hole array, following by polymerization under UV radiation. The silica/polymer composite can be easily peeled off from the hole array, and the embedded nanometer-scale silica colloids are removed to bring out an embroidered ball-like structure array.

To biomimic the size and shape of embroidered ball-like brochosomes, 450 nm silica colloidal suspensions with various colloid volume fractions are applied in the self-assembly process. The as-assembled close-packed monolayer silica colloidal crystals are partially embedded in the poly(PFPE-MAA) matrices (Fig. S2). It is worthwhile to note that the usage of suspensions with higher colloid volume fractions brings about less poly(PFPE-MAA)-embedded silica colloidal crystals. Importantly, the resulting hexagonally ordered poly(PFPE-MAA) hole arrays are well-retained after removing the templating silica colloids (Fig. S3). It is evident that the opening size increases with the colloid volume fraction of suspension. As the colloid volume fraction reaches 35 vol%, a maximum opening size can be achieved. Self-assembled 90 nm silica colloidal crystals are then deposited on the close-packed holes (*ca.* 450 nm in diameter of opening) (Fig. 3), followed by casting an ETPTA monomer/EGDA monomer mixture. After polymerization, the silica/polymer composites can be easily peeled off from the hole arrays to create close-packed raspberry-like structure arrays (Fig. 4), owing to low surface energy of poly(PFPE-MAA). The average diameters of monolayer 90 nm silica colloidal crystal-imbedded raspberry-like structures and multilayer 90 nm silica colloidal crystal-imbedded raspberry-like structures are *ca.* 450 nm, indicating that the structures are well preserved during the templating process. The embedded 90 nm silica colloids are finally wet-etched to design and build a close-packed artificial brochosome array. In comparison to featureless bumps (Fig. 5 (a) and (b)) templated from bare holes, bumps covered with nanometer-scale holes (Fig. 5 (c) and (d)) and embroidered ball-like structures (Fig. 5 (e) and (f)) are template from monolayer silica colloid crystal-deposited holes and multilayer silica colloid crystal-deposited holes, respectively. Although a few defects are noticed in Fig. 5, it is evident that the structure arrays are hexagonal close-packed. Importantly, various-sized/shaped hierarchical structures can be further developed by applying varied-sized colloids in the self-assembly procedure.
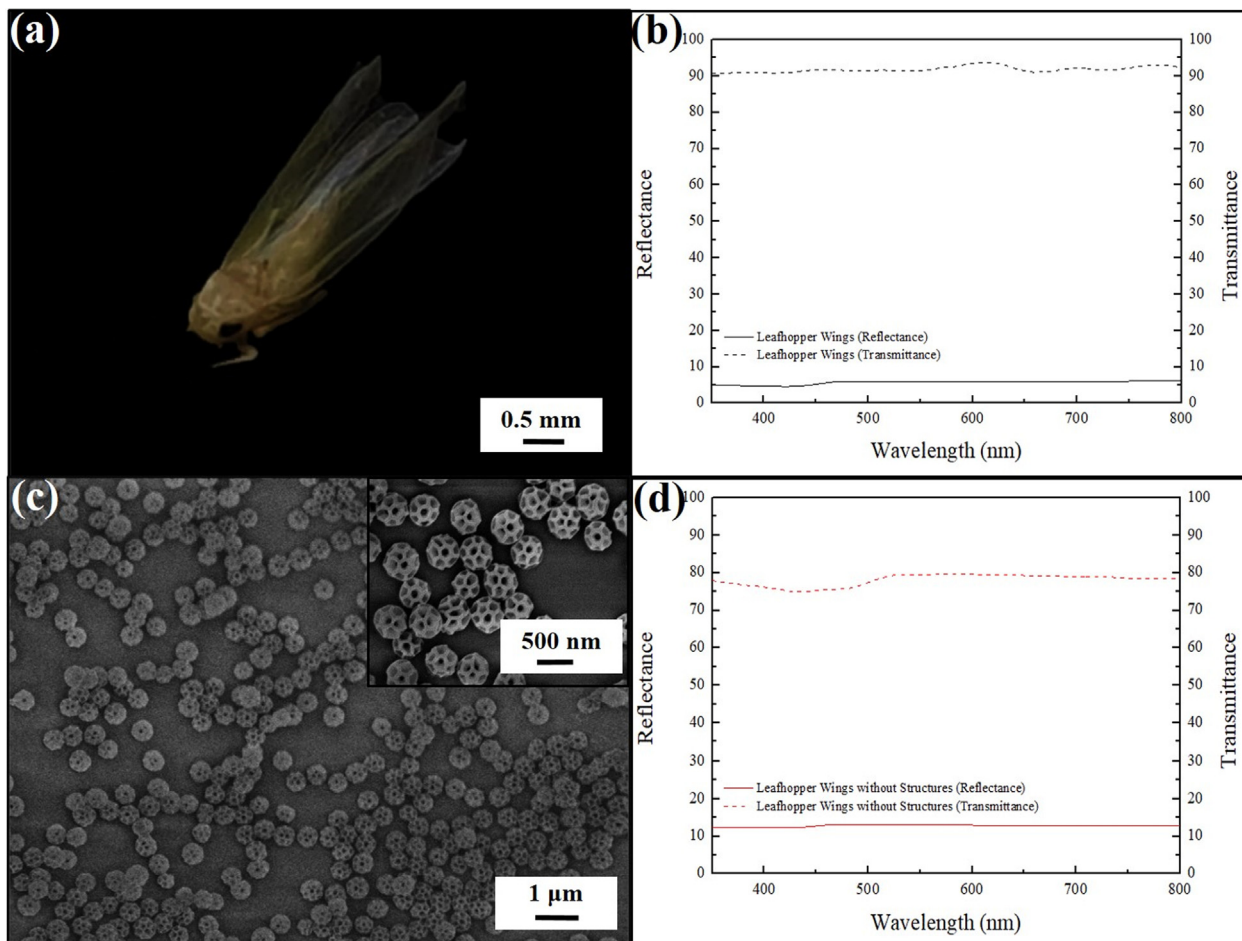
Fig. 1. (a) Photograph of a small yellow leafhopper under natural light illumination. (b) Reflectance and transmittance spectra in the visible spectral range at normal incidence acquired from the leafhopper wings. (c) Top-view SEM images of the leafhopper wings in (a). The insert shows a magnified SEM image. (d) Reflectance and transmittance spectra in the visible spectral range at normal incidence acquired from the leafhopper wings after removing the secretory brochosomes. (For interpretation of the references to color in this figure legend, the reader is referred to the web version of this article.)
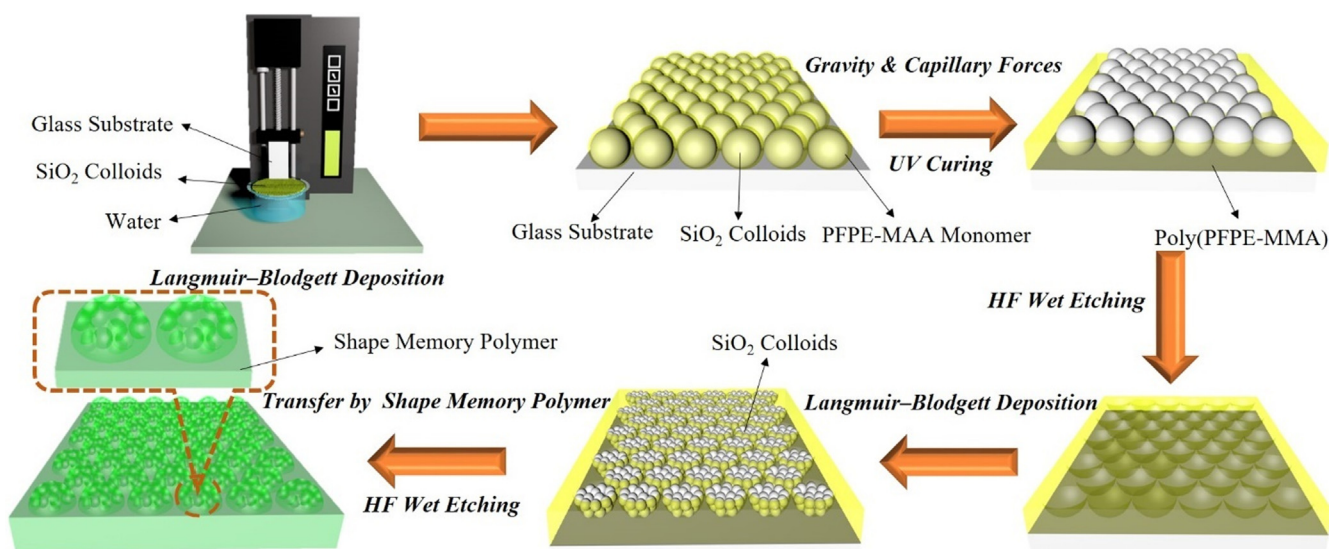

Fig. 2. Schematic illustration of the fabrication procedures for engineering embroidered ball-like antireflective structure arrays.

To investigate optical properties of the brochosome-inspired hierarchical structure arrays, reflectance and transmittance spectra of a bare poly(ETPTA)/poly(EGDA) film and the hierarchical structure-coated poly(ETPTA)/poly(EGDA) films are evaluated. The bare polymer film (black curves) displays an average reflectance of 12% (Fig. 6 (a)) and an average transmittance of 85%
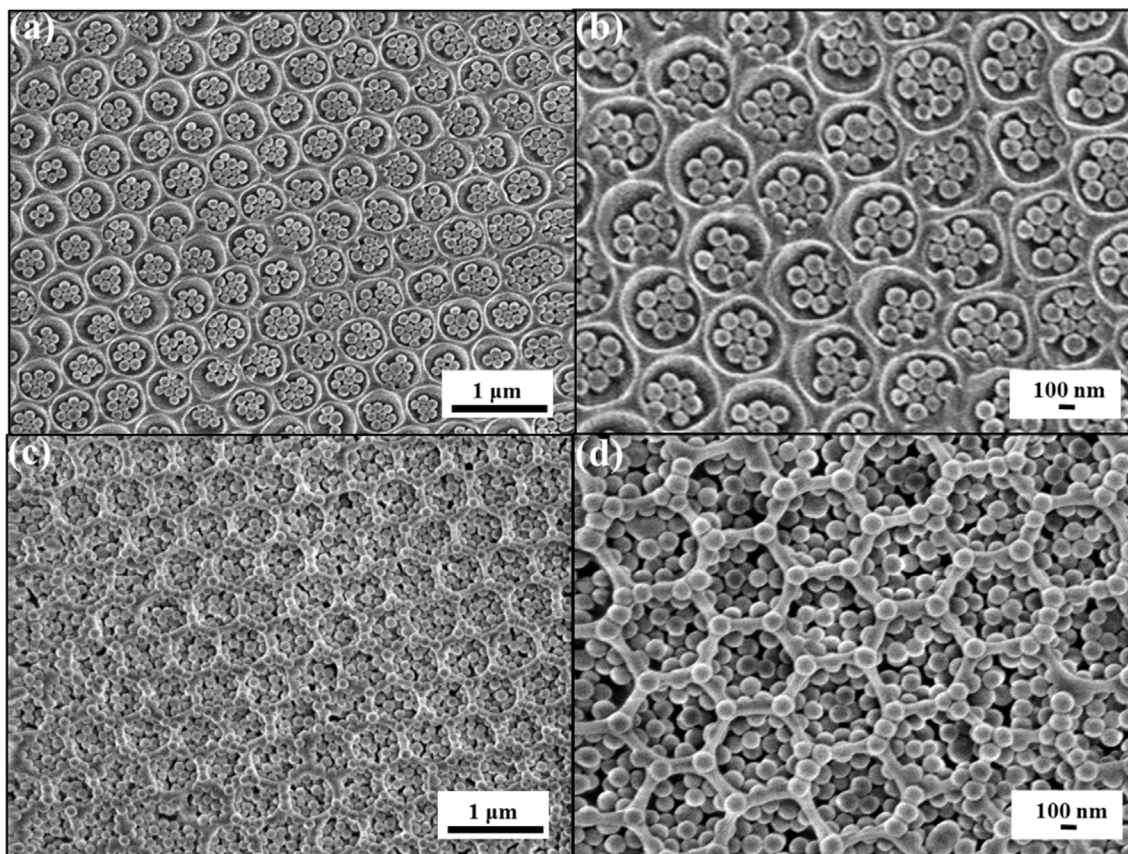
Fig. 3. Top-view SEM images of (a), (b) monolayer 90 nm silica colloidal crystals, and (c), (d) multilayer 90 nm silica colloidal crystals self-assembled onto close-packed hole arrays. The average hole depths are *ca.* 225 nm.
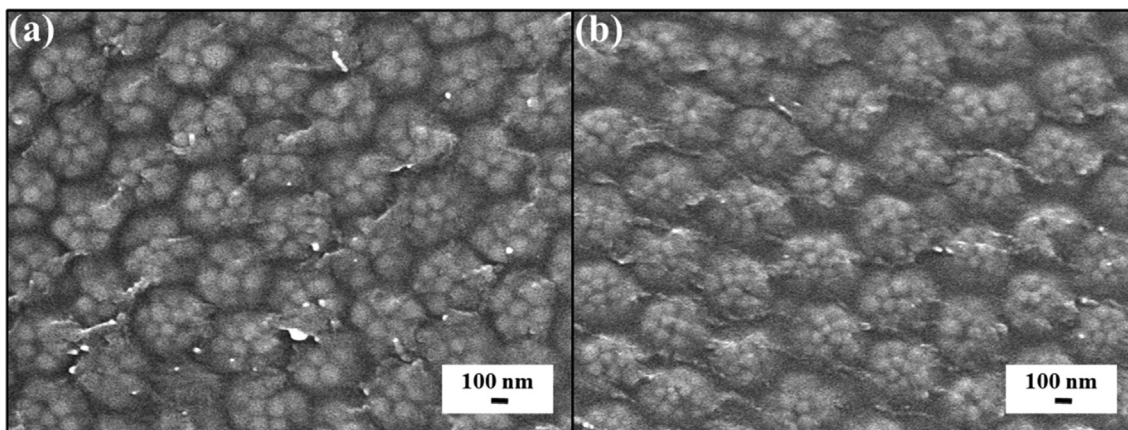

Fig. 4. Top-view SEM images of (a) close-packed raspberry-like structure arrays with monolayer 90 nm silica colloidal crystals embedded, and (b) close-packed raspberry-like structure arrays with multilayer 90 nm silica colloidal crystals embedded. The average structural heights are *ca.* 225 nm.

(Fig. 6 (b)) in visible spectra range, resulted from discontinue refractive index transition at the air/polymer interface. In comparison with that, the bump array-coated specimen (red curves) only exhibits a slightly lower reflectance and a slightly higher transmittance. Even though a gradual refractive index transition is established on the film surface, the bumps with *ca.* 225 nm in heights and *ca.* 450 nm in widths bring about light reflection and light refraction within the structures. It is worth noting that the light reflection and light refraction can be suppressed by introducing nanometer-scale holes (orange curves). Importantly, the average reflectance in visible spectra range of embroidered ball-like structure (*ca.* 225 nm in height) array-coated specimen reaches 6%,

while the average transmittance achieves 92% (red curves). The low reflectivity can be further comprehended by computing effective refractive index changes across the templated structure arrays using an effective medium theory (Fig. 6 (c)). On account of a lower average effective refractive index and a smoother effective refractive index transition, specular reflectance is reduced efficiently on the embroidered ball-like structure array-coated surface. Most importantly, the optical reflectances and transmittances of the aforementioned coatings present similar tendencies at various incident angles from 15°, 30°, 45°, 60° to 75° (Fig. S4). The broadband (visible) omnidirectional antireflective capability of the embroidered ball-like structures is even competitive with that of
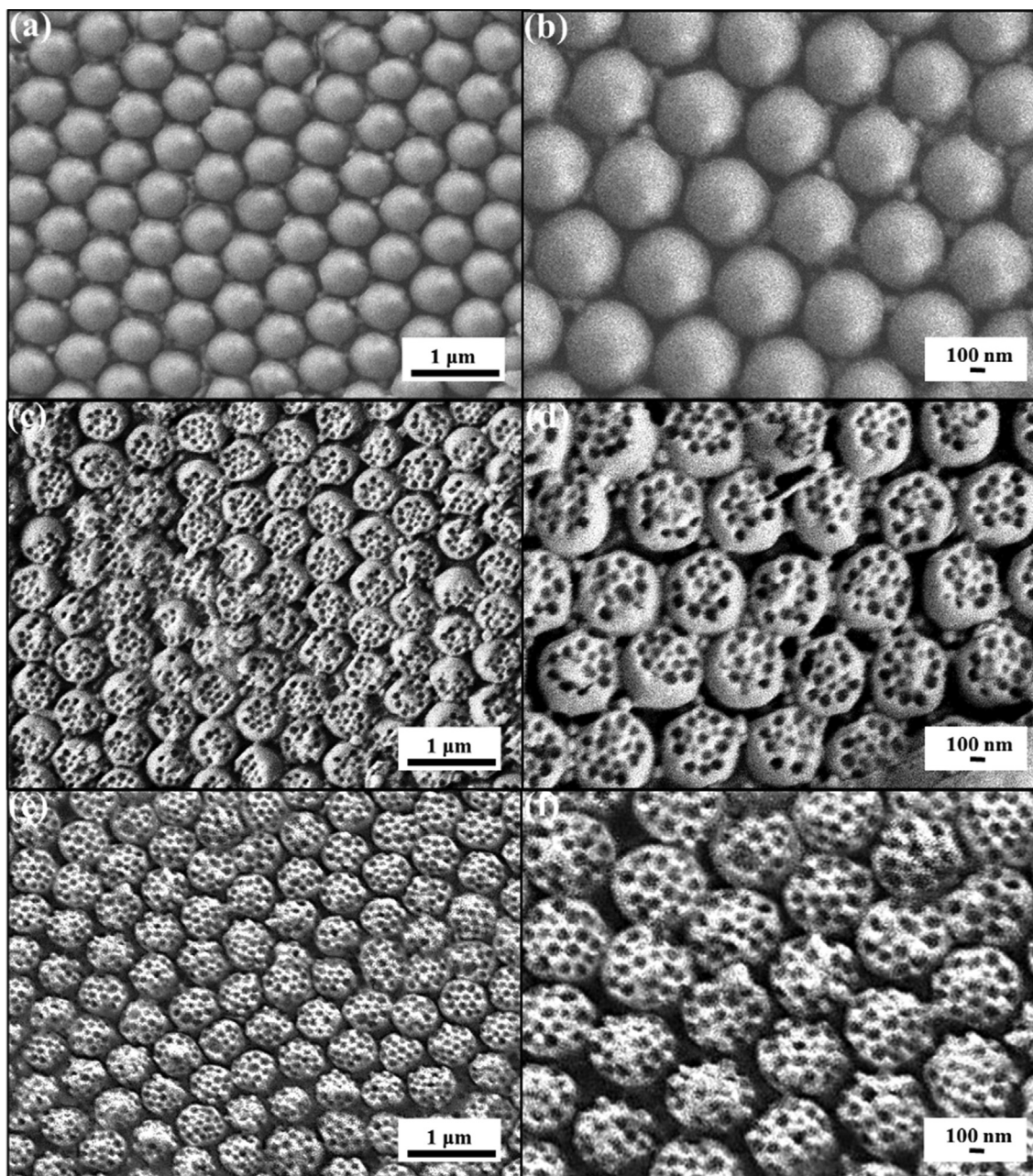
Fig. 5. Top-view SEM images of (a), (b) close-packed bump arrays, (c), (d) close-packed bump arrays covered with 90 nm holes, and (e), (f) close-packed embroidered ball-like structure arrays. The average structural heights are *ca.* 225 nm.

the brochosomes on leafhopper wings (Fig. S5). Moreover, photographs of a poly(ETPTA)/poly(EGDA) film with a square area coated with the embroidered ball-like structure array are carried out at various viewing angles (Fig. 6 (d), (e), and (f)). In contrast to the appearance of featureless area, the square area is uniform and highly transparent under white light illumination. The photographic images demonstrate once more that omnidirectional antireflective characteristics are improved by engineering embroidered ball-like structure arrays on surfaces.

Toward a better understanding of the antireflective structure-effect on antireflective characteristics at various incident angles, hierarchical structures are also templated from 300 nm hole arrays (Figs. S6, S7, and S8) and 450 nm hole arrays (Figs. S9, S10, and S11), respectively, following the fabrication procedures as reported previously. It is clear that the as-engineered hierarchical structures are hexagonally arranged (Figs. S12 and S13), though a few defects

are observed. Interestingly, average depth of the 300 nm hole arrays is *ca.* 150 nm (Fig. S8), thereby only single 90 nm silica colloid is available to be deposited on the hole in the first deposition procedure. The single colloid-deposited hole array can then serve as a template to create a single-hole-covered bump array (Fig. S12 (c) and (d)).

Average reflectances and average transmittances in visible spectral range of all the specimens mentioned above are evaluated from 0° to 75°, and summarized in Fig. 7. It is evident that light reflection at various incident angles can be suppressed by introducing the structure arrays. In addition, higher structure arrays bring about smoother effective refractive index transitions, resulting in lower average reflectances and higher average transmittances. It is worthwhile to notice that the structures with *ca.* 300 nm in heights and *ca.* 600 nm in widths exhibit strong light scattering and broadband light absorption (Fig. S14), leading to lowest average reflectances and
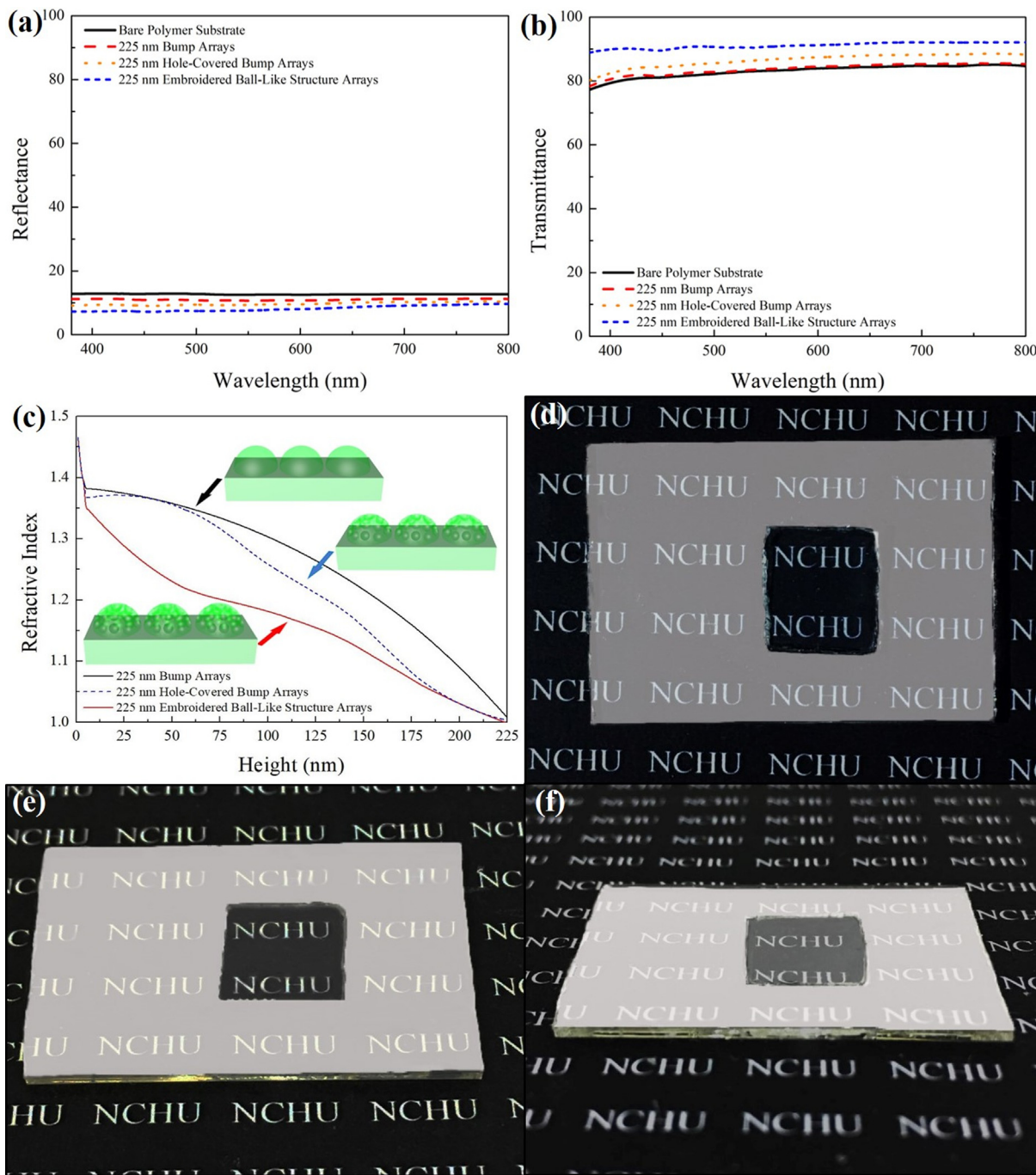
Fig. 6. (a) Reflectance and (b) transmittance spectra in visible spectral range at normal incidence acquired from a bare polymer substrate and polymer substrates coated with close-packed bump arrays, close-packed hole-covered bump arrays, and close-packed embroidered ball-like structure arrays. The average structural heights are *ca.* 225 nm. (c) The changes of computed effective refractive indexes from the bottom (height = 0 nm) to the top (height = 225 nm) of templated structure arrays. Photographs of a polymer substrate with a square area coated with the close-packed embroidered ball-like structure array at various viewing angles. (d) 0°, (e) 30°, and (f) 75°.

average transmittances (blue curves). Importantly, in comparison to the reflectance spectra and transmittance spectra of bump arrays and hole-covered bump arrays, low-reflectivity within a wide range of incident angles (+/-45°) can be achieved by establishing embroidered ball-like structure arrays. The visible light reflection on the embroidered ball-like structure (*ca.* 225 nm in height) array-coated specimen can be reduced by *ca.* 6% at 0° and *ca.* 20% at 75°, while the average transmittances of that are enhanced by *ca.* 7% at 0° and *ca.* 17% at 75° (orange curves).

The poly(ETPTA)/poly(EGDA) copolymer utilized in this research is with a glass transition temperature of about −42 °C, and possesses shape memory characteristics at room temperature [53]. Owing to the unique feature, the embroidered ball-like structure (*ca.* 225 nm in height) array can be deformed after submerging in water, followed by drying out of water in ambient environment (Fig. 8 (a)). During water evaporation, the high capillary pressure induced by water surface tension is capable of overcoming intermolecular interactions within the shape memory copolymer, and therefore squeezing the templated embroidered ball-like structures. The resulting light scattering and light reflection from the squeezed structures lead to low transmittances at various incidence angles. Interestingly, the temporarily deformed structures are recovered by exposing the
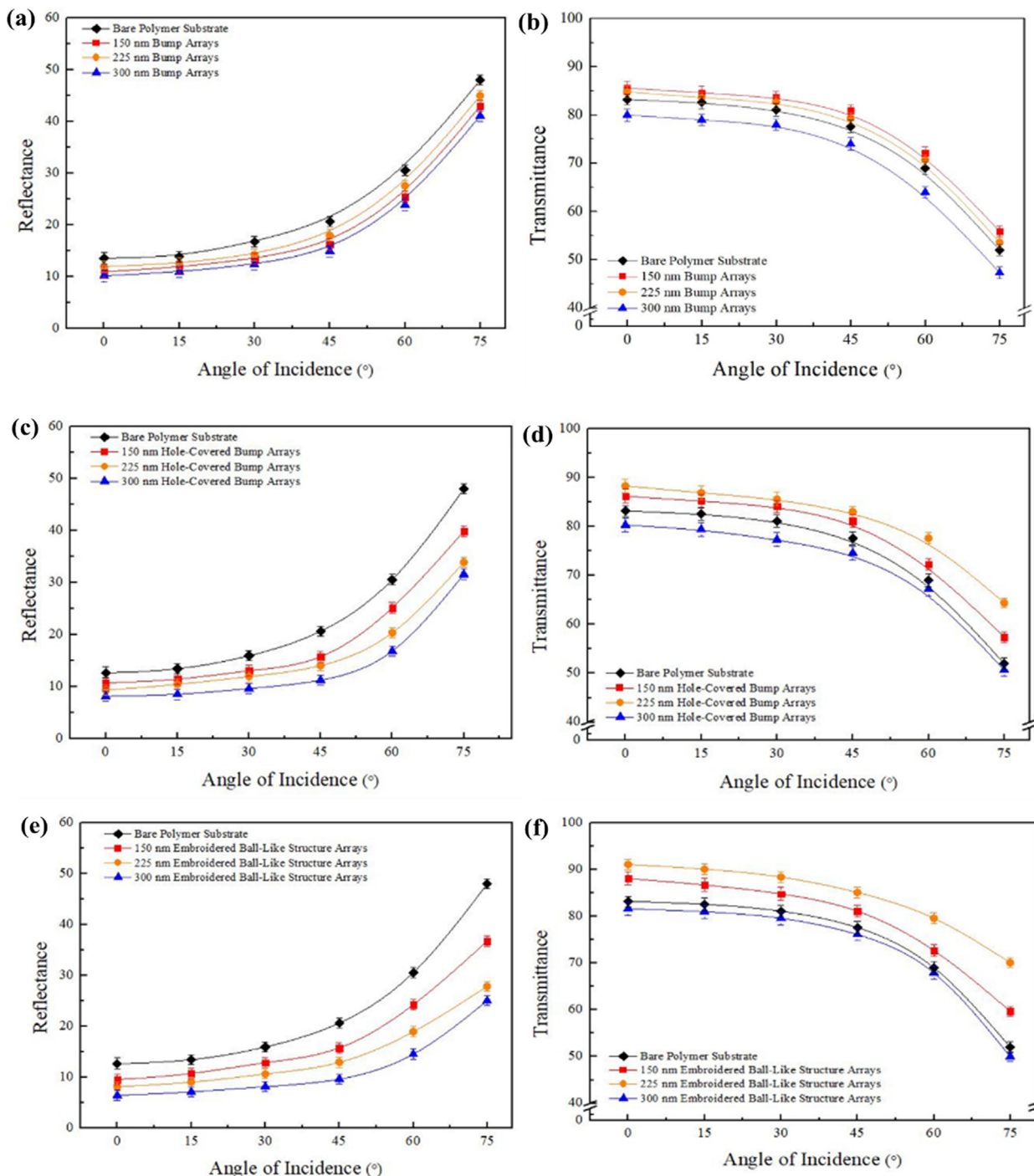
Fig. 7. Average reflectances and average transmittances in visible spectral range at various incidence angles acquired from a bare polymer substrate and polymer substrates coated with (a), (b) close-packed bump arrays, (c), (d) close-packed hole-covered bump arrays, and (e), (f) close-packed embroidered ball-like structure arrays.

specimen to low surface tension liquids such as ethanol, which can swell the copolymer (Fig. 8 (b)). The low surface tensions lead to low capillary forces during drying, which are not as much as required to squeeze the structures. Associated with the structural transitions, broadband (visible) antireflective characteristics of the embroidered ball-like structure array can be accurately triggered in seconds by applying demanded solvent drying procedures (Fig. 8 (c) and (d)). Another distinct behavior of the shape-memory-enabled antireflective structures is that the highly transparent appearance is reversible by repeating the water drying and ethanol drying procedures. The average transmittance at normal incidence can be switched between

92% and 84% even after repeated 25 capillary force-induced deforming/recovering cycles (Fig. 8 (e)). It is apparent that the deformed structure array-coated specimen (left half) exhibits a pale white appearance, while the recovered structure array-coated specimen (right half) is highly transparent after 25 deforming/recovering cycles (Fig. 8 (f)). The results further demonstrate that the shape memory effect presented by the embroidered ball-like structure array is well-preserved during the cyclic operations at room temperature.

More interestingly, temporarily deformed structures can also be recovered into inherent ordered structures instantaneously by
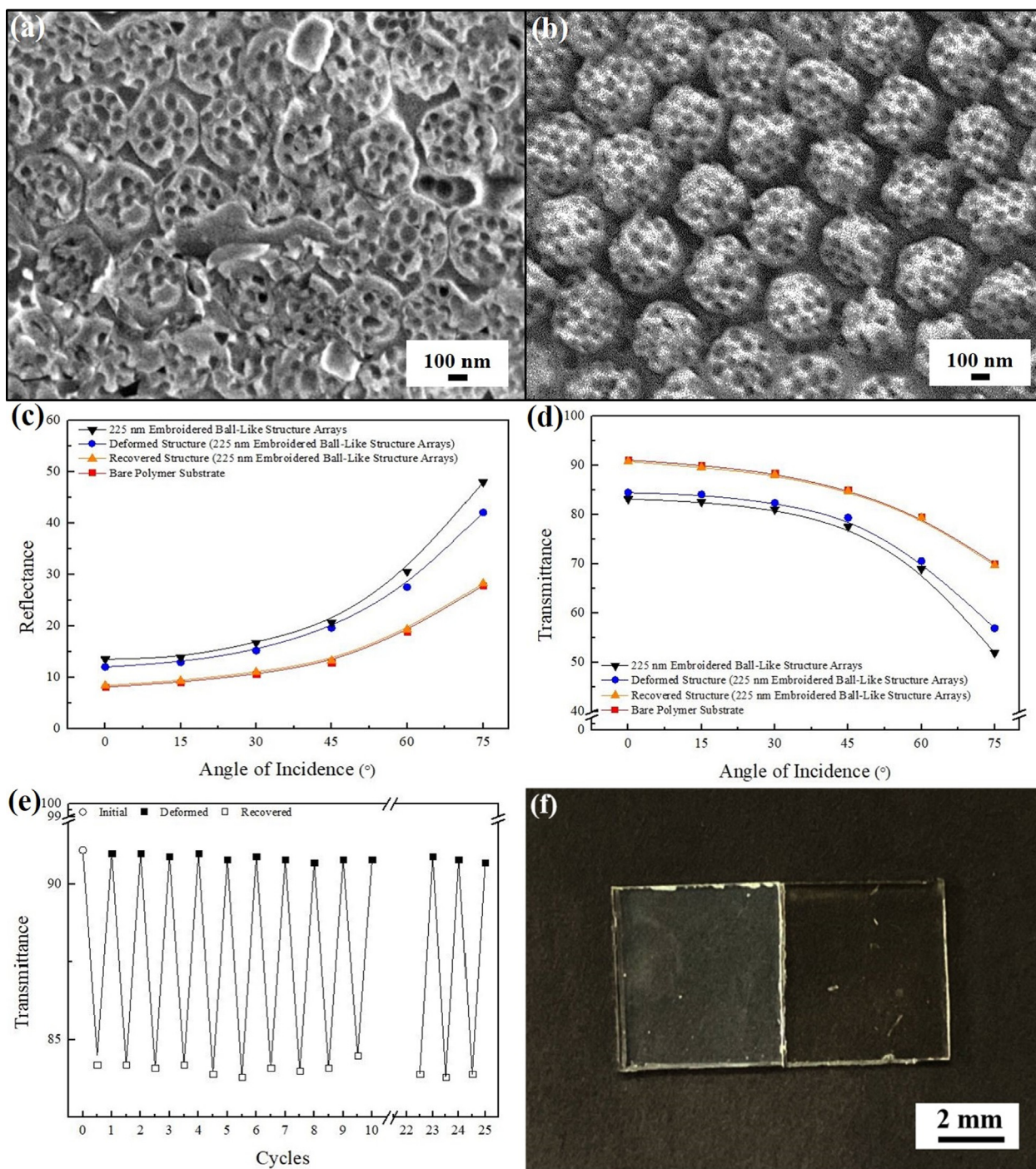
Fig. 8. Top-view SEM images of (a) deformed and (b) recovered close-packed embroidered ball-like structure arrays. The intrinsic average structural heights are *ca.* 225 nm. (c) Average reflectances and (d) average transmittances in visible spectral range at various incidence angles acquired from deformed close-packed embroidered ball-like structure arrays after applying an ethanol drying procedure. (e) Reversible antireflection functionality of the close-packed embroidered ball-like structure arrays enabled by applying an ethanol drying procedure. (f) Photograph of a polymer substrate with left half coated with deformed structure arrays and right half coated with recovered structure arrays after 25 deforming/recovering cycles.

applying contact pressures. To verify that, demanded standard calibration weights are placed on the squeezed structures in a selected area, on which is covered with a piece of cover glass. After gently lifting up the weights, the squeezed structures are recovered, which is attributed to attractive van der Waals forces between the cover glass and the structures. The recovered structures after applying various contact pressures are presented in Fig. S15. It is evident that applying of a higher contact pressure leads to a further recovery of demanded structures, and the

embroidered ball-like structure array can be fully recovered as the contact pressure reaches 2.94 N/cm². To evaluate the corresponding antireflective characteristics of the deformed structure arrays after applying various contact pressures, average reflectances and average transmittances in visible spectral range of the specimens are acquired at various incidence angles (Fig. 9 (a) and (b)). It is found that the deformed structure array under higher contact pressure exhibits an improved antireflection performance. Furthermore, the reflectance and transmittance of the fully-
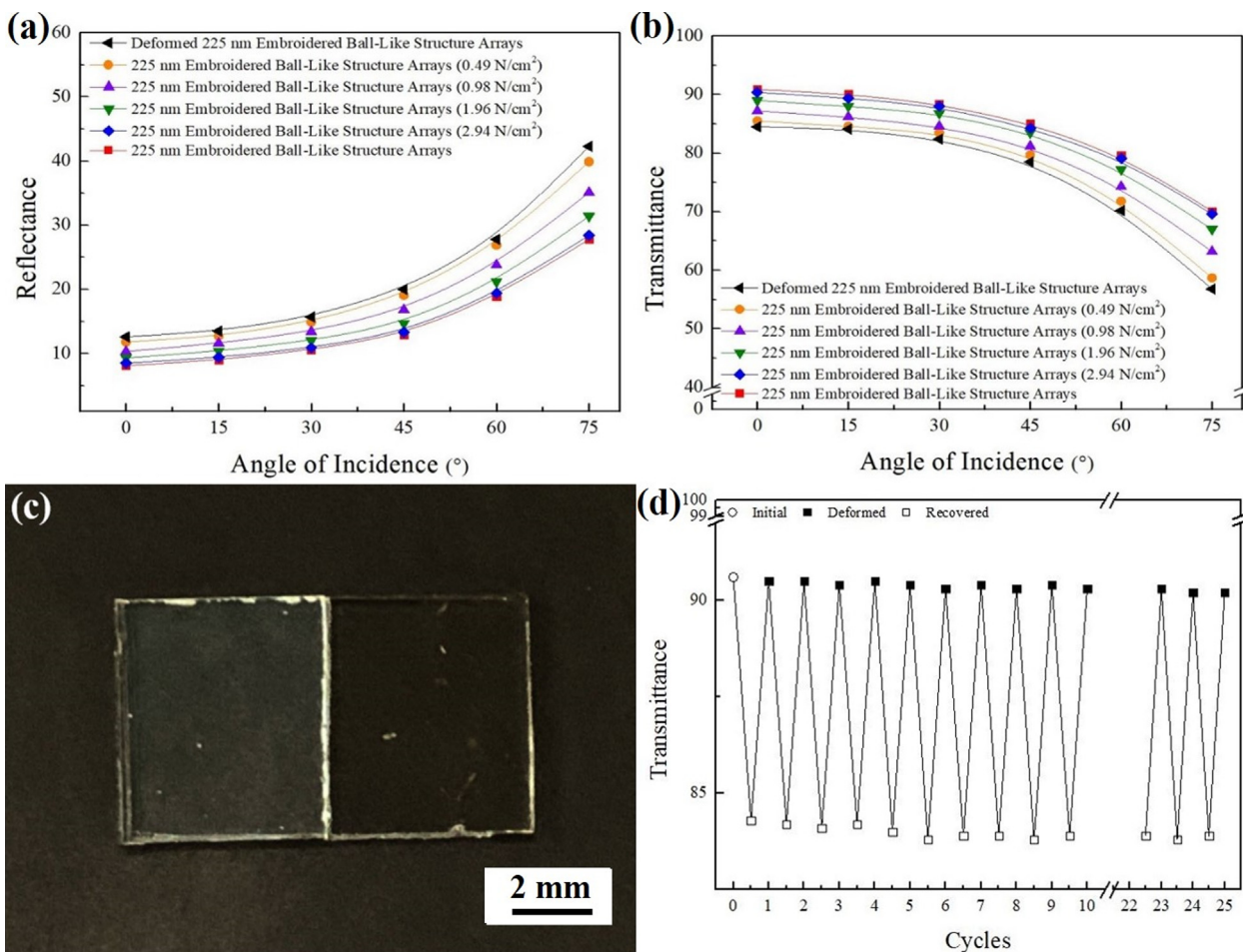
Fig. 9. (a) Average reflectances and (b) average transmittances in visible spectral range at various incidence angles acquired from deformed close-packed embroidered ball-like structure arrays after applying various pressures. The intrinsic average structural heights are *ca.* 225 nm. (c) Photograph of a polymer substrate with left half coated with deformed structure arrays and right half coated with recovered structure arrays. (d) Reversible antireflection functionality of the close-packed embroidered ball-like structure arrays enabled by applying pressure.

recovered structure array (2.94 N/cm^2 contact pressure) agree well with those of the undamaged structure array. The results indicate that the broadband (visible) antireflective capability of the as-engineered shape-memory embroidered ball-like structure array can be restored by applying a contact pressure of 2.94 N/cm^2.

As confirmed earlier, the restored antireflective characteristics can be erased once again by introducing capillary forces in a water drying procedure (Fig. 9 (c)). The contact pressure-induced cyclic shape memory operations are reversible for more than 25 cycles (Fig. 9 (d)). Importantly, varying degrees of antireflection performances can also be reversibly triggered by applying various contact pressures (Fig. S16).

4. Conclusions

To conclude, stimuli-responsive antireflective structures are engineered through combining a modified Langmuir-Blodgett technique and a templating method. The resulting close-packed embroidered-ball like hierarchical structure array, inspired by leafhopper-generated brochosomes, is capable of suppressing visible light reflection for wide incidence angles. Importantly, the broadband (visible) low-reflectivity within a wide range of incident angles can be erased by temporally squeezing the structures utilizing capillary forces induced by water evaporation. Owing to the shape memory behaviors, the structures can be recovered by drying out of ethanol or by applying required contact pressures

under ambient conditions for regenerating highly transparent appearances. The reversible omnidirectional antireflective characteristics, associated with repeatable structure deforming/recovering cycles, provide a platform in developing various smart optical devices.

CRediT authorship contribution statement

Pei-Chun Li: Methodology, Validation, Investigation, Resources, Writing - original draft. **Huei-Yin Chen:** Software, Investigation, Visualization. **Kuan-Ting Chiang:** Software, Investigation, Resources. **Hongta Yang:** Conceptualization, Writing - review & editing, Supervision, Project administration, Funding acquisition.

Declaration of Competing Interest

The authors declare that they have no known competing financial interests or personal relationships that could have appeared to influence the work reported in this paper.

Acknowledgments

References

[1] J.-Q. Xi, M.F. Schubert, J.K. Kim, E.F. Schubert, M. Chen, S.-Y. Lin, W. Liu, J.A. Smart, Optical Thin-Film Materials with Low Refractive Index for Broadband Elimination of Fresnel Reflection, Nat. Photonics 1 (2007) 176–179.

[2] J. Li, J. Zhu, X. Gao, Bio-Inspired High-Performance Antireflection and Antifogging Polymer Films, Small 10 (2014) 2578–2582.

[3] Y. Zhu, L. Chen, C. Zhang, Z. Guan, Preparation of Hydrophobic Antireflective SiO2 Coating with Deposition of PDMS From Water-Based SiO2-PEG Sol, Appl. Surf. Sci. 457 (2018) 522–528.

[4] K. Askar, B.M. Phillips, Y. Fang, B. Choi, N. Gozubenli, P. Jiang, B. Jiang, Self-Assembled Self-Cleaning Broadband Anti-Reflection Coatings, Colloids Surf., A 439 (2013) 84–100.

[5] J.-Q. Xi, M. Ojha, W. Cho, J. Plawsky, W. Gill, T. Gessmann, E. Schubert, Omnidirectional Reflector Using Nanoporous SiO2 as a Low-Refractive-Index Material, Opt. Lett. 30 (2005) 1518–1520.

[6] D. Berman, S. Guha, B. Lee, J.W. Elam, S.B. Darling, E.V. Shevchenko, Sequential Infiltration Synthesis for the Design of Low Refractive Index Surface Coatings with Controllable Thickness, ACS Nano 11 (2017) 2521–2530.

[7] K. Pfeiffer, L. Ghazaryan, U. Schulz, A. Szeghalmi, Wide-Angle Broadband Antireflection Coatings Prepared by Atomic Layer Deposition, ACS Appl. Mater. Interfaces 11 (2019) 21887–21894.

[8] P. Löbmann, Antireflective Coatings by Sol-Gel Processing: Commercial Products and Future Perspectives, J. Sol-Gel Sci. Technol. 83 (2017) 291–295.

[9] B.-T. Liu, W.-D. Yeh, Antireflective Surface Fabricated from Colloidal Silica Nanoparticles, Colloids Surf., A 356 (2010) 145–149.

[10] J.Y.Y. Loh, N. Kherani, Design of Nano-Porous Multilayer Antireflective Coatings, Coatings 7 (2017) 134.

[11] Y. Du, L.E. Luna, W.S. Tan, M.F. Rubner, R.E. Cohen, Hollow Silica Nanoparticles in UV-Visible Antireflection Coatings for Poly(methyl methacrylate) Substrates, ACS Nano 4 (2010) 4308–4316.

[12] E. Osorio, R. Urteaga, L.N. Acquaroli, G. García-Salgado, H. Juaréz, R.R. Koropecki, Optimization of Porous Silicon Multilayer as Antireflection Coatings for Solar Cells, Sol. Energy Mater. Sol. Cells 95 (2011) 3069–3073.

[13] P. Buskens, M. Burghoorn, M.C.D. Mourad, Z. Vroon, Antireflective Coatings for Glass and Transparent Polymers, Langmuir 32 (2016) 6781–6793.

[14] Z. Han, Z. Wang, B. Li, X. Feng, Z. Jiao, J. Zhang, J. Zhao, S. Niu, L. Ren, Flexible Self-Cleaning Broadband Antireflective Film Inspired by the Transparent Cicada Wings, ACS Appl. Mater. Interfaces 11 (2019) 17019–17027.

[15] Y. Zeng, X. Chen, Z. Yi, Y. Yi, X. Xu, Fabrication of Pn Heterostructure ZnO/Si Moth-Eye Structures: Antireflection, Enhanced Charge Separation and Photocatalytic Properties, Appl. Surf. Sci. 441 (2018) 40–48.

[16] A. Papadopoulos, E. Skoulas, A. Mimidis, G. Perrakis, G. Kenanakis, G.D. Tsibidis, E. Stratakis, Biomimetic Omnidirectional Antireflective Glass via Direct Ultrafast Laser Nanostructuring, Adv. Mater. 31 (2019) 1901123.

[17] Y. Lee, K. Koh, H. Na, K. Kim, J.-J. Kang, J. Kim, Lithography-Free Fabrication of Large Area Subwavelength Antireflection Structures Using Thermally Dewetted Pt/Pd Alloy Etch Mask, Nanoscale Res. Lett. 4 (2009) 364–370.

[18] K. Choi, S.H. Park, Y.M. Song, Y.T. Lee, C.K. Hwangbo, H. Yang, H.S. Lee, Nano-Tailoring the Surface Structure for the Monolithic High-Performance Antireflection Polymer Film, Adv. Mater. 22 (2010) 3713–3718.

[19] P. Fan, B. Bai, M. Zhong, H. Zhang, J. Long, J. Han, W. Wang, G. Jin, General Strategy Toward Dual-Scale-Controlled Metallic Micro-Nano Hybrid Structures with Ultralow Reflectance, ACS Nano 11 (2017) 7401–7408.

[20] K. Nishioka, T. Sueto, N. Saito, Formation of Antireflection Nanostructure for Silicon Solar Cells Using Catalysis of Single Nano-Sized Silver Particle, Appl. Surf. Sci. 255 (2009) 9504–9507.

[21] C. Yao, Y. Ye, B. Jia, Y. Li, R. Ding, Y. Jiang, Y. Wang, X. Yuan, Polarization and Fluence Effects in Femtosecond Laser Induced Micro/Nano Structures on Stainless Steel with Antireflection Property, Appl. Surf. Sci. 425 (2017) 1118–1124.

[22] K.-C. Park, H.J. Choi, C.-H. Chang, R.E. Cohen, G.H. Mckinley, G. Barbastathis, Nanotextured Silica Surfaces with Robust Superhydrophobicity and Omnidirecyional Broadband Supertransmissivity, Journal of Science: ACS Nano 6 (2012) 3789–3799.

[23] E. Stratakis, J. Bonse, J. Heitz, J. Siegel, G.D. Tsibidis, E. Skoulas, A. Papadopoulos, A. Mimidis, A.-C. Joel, P. Comanns, J. Krüger, C. Florian, Y. Fuentes-Edfud, J. Solis, W. Baumgartner, Laser Engineering of Biomimetic Surfaces, Mater. Sci. Eng. R 141 (2020) 100562.

[24] K.T. Tran, T.D. Nguyen, Lithography-Based Methods to Manufacture Biomaterials at Small Scales, J. Sci.: Adv. Mater. Devices 2 (2017) 1–14.

[25] D. Morphew, J. Shaw, C. Avins, D. Chakrabarti, Programming Hierarchical Self-Assembly of Patchy Particles into Colloidal Crystals *via* Colloidal Molecules, ACS Nano 12 (2018) 2355–2364.

[26] Z.M. Sherman, J.W. Swan, Transmutable Colloidal Crystals and Active Phase Separation via Dynamic, Directed Self-Assembly with Toggled External Fields, ACS Nano 13 (2019) 764–771.

[27] T. Ren, J. He, Substrate-Versatile Approach to Robust Antireflective and Superhydrophobic Coatings with Excellent Self-Cleaning Property in Varied Environments, ACS Appl. Mater. Interfaces 9 (2017) 34367–34376.

[28] P. Yu, C.H. Chang, C.H. Chiu, C.S. Yang, J.C. Yu, H.C. Kuo, S.H. Hsu, Y.C. Chang, Efficiency Enhancement of GaAs Photovoltaics Employing Antireflective Indium Tin Oxide Nanocolumns, Adv. Mater. 21 (2009) 1618–1621.

[29] R. Rakitov, S.N. Gorb, Brochosomes Protect Leafhoppers (Insecta, Hemiptera, Cicadellidae) from Sticky Exudates, J. R. Soc. Interface 10 (2013) 20130445.

[30] G.S. Watson, J.A. Watson, B.W. Cribb, Diversity of Cuticular Micro-and Nanostructures on Insects: Properties, Functions, and Potential Applications, Annu. Rev. Entomol. 62 (2017) 185–205.

[31] S. Yang, N. Sun, B.B. Stogin, J. Wang, Y. Huang, T.-S. Wong, Ultra-Antireflective Synthetic Brochosomes, Nature Commun. 8 (2017) 1–8.

[32] F.T. Chi, D.J. Liu, H.Y. Wu, J.H. Lei, Mechanically Robust and Self-Cleaning Antireflection Coatings from Nanoscale Binding of Hydrophobic Silica Nanoparticles, Sol. Energy Mater. Sol. Cells 200 (2019) 109939.

[33] C. Garlisi, E. Trepci, X. Li, R. Al Sakkaf, K. Al-Ali, R.P. Nogueira, L.X. Zheng, E. Azar, G. Palmisano, Multilayer Thin Film Structures for Multifunctional Glass: Self-Cleaning, Antireflective and Energy-Saving Properties, Appl. Energy 264 (2020) 114697.

[34] A.S. Sarkin, N. Ekren, S. Saglam, A Review of Anti-Reflection and Self-Cleaning Coatings on Photovoltaic Panels, Sol. Energy 199 (2020) 63–73.

[35] J. Hiller, J.D. Mendelsohn, M.F. Rubner, Reversibly Erasable Nanoporous Anti-Reflection Coatings from Polyelectrolyte Multilayers, Nat. Mater. 1 (2002) 59–63.

[36] X. Li, X.H. Yu, Y.C. Han, Intelligent Reversible Nanoporous Antireflection Film by Solvent-Stimuli-Responsive Phase Transformation of Amphiphilic Block Copolymer, Langmuir 28 (2012) 10584–10591.

[37] F.H. Zhang, Y.L. Xia, Y.J. Liu, J.S. Leng, Nano/Microstructures of Shape Memory Polymers: from Materials to Applications, Nanoscale Horiz. 5 (2020) 1155–1173.

[38] N. Yenpech, V. Intasanta, K. Tashiro, S. Chirachanchai, Color and Shape Reversible, Recoverable and Repeatable Mechanochromic Shape Memory Polycaprolactone: a Single Material with Dual Functions, Polym. Chem. 11 (2020) 91–101.

[39] S. Schauer, J.J. Baumberg, H. Holscher, S.K. Smoukov, Tuning of Structural Colors Like a Chameleon Enabled by Shape-Memory Polymers, Macromol. Rapid Commun. 39 (2018) 1800518.

[40] L. Sun, T.X. Wang, H.M. Chen, A.V. Salvekar, B.S. Naveen, Q.W. Xu, Y.W. Weng, X.L. Guo, Y.H. Chen, W.M. Huang, A Brief Review of the Shape Memory Phenomena in Polymers and Their Typical Sensor Applications, Polymers 11 (2019) 1049.

[41] H.B. Lu, Y.T. Yao, L. Lin, Temperature Sensing and Actuating Capabilities of Polymeric Shape Memory Composite Containing Thermochromic Particles, Pigm. Resin Technol. 44 (2015) 224–231.

[42] L.B. Wang, K.S. Xiong, Z.B. Wang, A Novel Heat-Triggered Shape-Memory Polymer Based on Ethylene-Vinyl Acetate Copolymer/Nitrile-Butadiene Rubber Thermoplastic Vulcanizates, J. Thermoplast. Compos. Mater. 33 (2020) 1217–1233.

[43] A.J. Boyle, A.C. Weems, S.M. Hasan, L.D. Nash, M.B.B. Monroe, D.J. Maitland, Solvent Stimulated Actuation of Polyurethane-Based Shape Memory Polymer Foams Using Dimethyl Sulfoxide and Ethanol, Smart Mater. Struct. 25 (2016) 075014.

[44] K. Yu, K.K. Westbrook, P.H. Kao, J.S. Leng, H.J. Qi, Design Considerations for Shape Memory Polymer Composites with Magnetic Particles, J. Compos. Mater. 47 (2013) 51–63.

[45] W. Al Azzawi, J.A. Epaarachchi, J.S. Leng, Investigation of Ultraviolet Radiation Effects on Thermomechanical Properties and Shape Memory Behaviour of Styrene-Based Shape Memory Polymers and its Composite, Compos. Sci. Technol. 165 (2018) 266–273.

[46] F. Xie, L.W. Liu, X.B. Gong, L.N. Huang, J.S. Leng, Y.J. Liu, Effects of Accelerated Aging on Thermal, Mechanical and Shape Memory Properties of Cyanate-Based Shape Memory Polymer: I Vacuum Ultraviolet Radiation, Polym. Degrad. Stab. 138 (2017) 91–97.

[47] W. Stöber, A. Fink, E. Bohn, Controlled Growth of Monodisperse Silica Spheres in the Micron Size Range, J. Colloid Interface Sci. 26 (1968) 62–69.

[48] C.-W. Lei, R.-Y. Chen, H. Yang, Leafhopper Wing-Inspired Broadband Omnidirectional Antireflective Embroidered Ball-Like Structure Arrays Using a Nonlithography-Based Methodology, Langmuir 36 (2020) 5296–5302.

[49] K. Li, P. Berton, S.P. Kelley, R.D. Rogers, Singlet Oxygen Production and Tunable Optical Properties of Deacetylated Chitin-Porphyrin Crosslinked Films, Biomacromolecules 19 (2018) 3291–3300.

[50] S. Dhananasekaran, R. Palanivel, S. Pappu, Adsorption of Methylene Blue, Bromophenol Blue, and Coomassie Brilliant Blue by α-Chitin Nanoparticles, J. Adv. Res. 7 (2016) 113–124.

[51] T. Kohoutek, M. Parchine, M. Bardosova, M.E. Pemble, Controlled Self-Assembly of Langmuir-Blodgett Colloid Crystal Films of Monodispersed Silica Particles on Non-Planar Substrates, Colloids Surf., A 593 (2020) 12465.

[52] H. Jeong, H. Liangbing, H.R. Lee, E. Garnett, J.W. Choi, C. Yi, Fast and Scalable Printing of Large Area Monolayer Nanoparticles for Nanotexturing Applications, Nano Lett. 10 (2010) 2989–2994.

[53] C.J. Leverant, S.-Y. Leo, M.A. Cordoba, Y. Zhang, N. Charpota, C. Taylor, P. Jiang, Reconfigurable Anticounterfeiting Coatings Enabled by Macroporous Shape Memory Polymers, ACS Appl. Polym. Mater. 1 (2018) 36–46.